Efficient Luminescent Down-Shifting Detectors Based on Colloidal Quantum Dots for Dual-Band Detection Applications

Scott M. Geyer,[†] Jennifer M. Scherer,[†] Nosipho Moloto,[†] Frank B. Jaworski,[‡] and Moungi G. Bawendi[†,*]

[†]Department of Chemistry, Massachusetts Institute of Technology, Cambridge, Massachusetts 02139, United States, and [‡]Raytheon Vision Systems, Goleta, California, United States

ABSTRACT A colloidal quantum dot (QD) luminescent down-shifting (LDS) layer is used to sensitize an InGaAs short wavelength infrared photodetector to the near UV spectral band. An average improvement in the external quantum efficiency (EQE) from 1.8% to 21% across the near UV is realized using an LDS layer consisting of PbS/CdS core/shell QDs embedded in PMMA. A simple model is used to fit the experimental EQE data. A UV sensitive InGaAs imaging array is demonstrated and the effect of the LDS layer on the optical resolution is calculated. The bandwidth of the LDS detector under UV illumination is characterized and shown to be determined by the photoluminescence lifetime of the QDs.

KEYWORDS: dual-band · down-shifting · quantum dot · nanocrystal · SWIR · InGaAs

Modern p-n junction photodetectors are designed to operate with high efficiency across a specific band of the electromagnetic spectrum. Photons with energy below the detector band gap are not absorbed and photons with energy far greater than the band gap are absorbed near the surface of the detector and are not collected efficiently.[1] For a number of applications the capability to detect two or more bands simultaneously with a single imaging system is of interest.[2−5] This can be achieved by luminescent down-shifting (LDS) of photons with energy above the detector band using fluorescent dyes[1,6] or colloidal quantum dots (QD).[7,8] A layer incorporating the fluorophore is deposited above the detector and absorbs high energy photons. After electronic and vibrational relaxation, the down-shifted photons are re-emitted in the detector band. This method has been demonstrated for UV−vis down-shifting to enhance solar cell efficiency using organic dyes.[1,6]

In this paper we demonstrate the application of colloidal quantum dots to sensitize short wavelength infrared (SWIR) detectors to ultraviolet light. UV−SWIR dual-band detectors have applications in flame identification for fire fighting, communications, muzzle flash identification, and covert tagging.[2,3] We demonstrate that the unique absorption profile and high quantum yield (QY) of QDs make these particles ideal candidates for LDS emitters in UV−SWIR applications and dual-band detectors in general.

BACKGROUND

Figure 1 depicts the operation of a QD-based UV−SWIR LDS detector. Incident infrared light is collected with high efficiency by the bare detector. Higher energy UV light is absorbed near the detector surface, not in the active region of the p−n junction detector. Surface states and a low minority carrier diffusion length result in a low internal quantum efficiency and therefore poor sensitivity to visible and ultraviolet light.[1,2] In the LDS detector geometry, a layer containing luminescent QDs is deposited on the bare detector. Ultraviolet light is absorbed by the QDs and re-emitted in the infrared region where it is collected with high efficiency by the SWIR detector. The QDs absorb more strongly in the UV than the SWIR, allowing the LDS layer to be highly transparent across the detector band.

RESULTS

External Quantum Efficiency. The absorption and emission spectra of PbS/CdS core/shell QDs in solution are shown in Figure 2 overlaid with the external quantum efficiency of an InGaAs short wavelength infrared (SWIR) detector.[9] The size of the QD core is chosen so that the emission overlaps with the high efficiency region of the SWIR detector. The CdS shell is added to improve the air

* Address correspondence to mgb@mit.edu.

Received for review March 17, 2011 and accepted May 17, 2011.

Published online May 17, 2011
10.1021/nn2010238

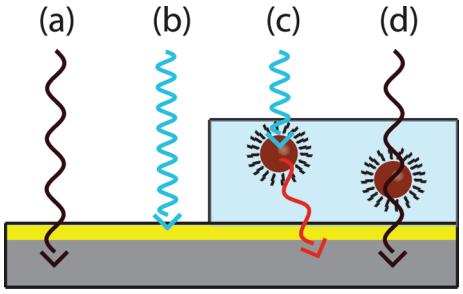

Figure 1. Cartoon of a QD sensitized UV–SWIR LDS detector. (a) SWIR light is collected in the active region of the bare InGaAs detector (gray box). (b) UV light is collected near the surface of the bare detector (yellow box) at low efficiency. (c) With the addition of the LDS layer, UV light is absorbed by the QDs and re-emitted in the SWIR where it is collected in the active region of the detector. (d) The QDs absorb strongly in the UV but weakly in the SWIR.

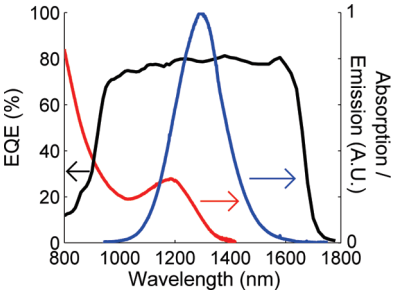

Figure 2. The absorption (red line) and emission (blue line) spectra of PbS/CdS QDs in solution are shown compared to the EQE of an InGaAs SWIR detector (black line).

stability of the QDs and also serves to increase absorption in the UV.

The quantum yield (QY) of the PbS/CdS QDs in solution is 55% as measured with an integrating sphere. However, in a thin film of close packed QDs the QY is reduced to less than 10% due to fluorescence resonant energy transfer (FRET) between QDs. FRET transfer in close packed QD films reduces the overall film QY *via* transfer of excitons from QDs with high QY to QDs with low QY.[10,11] To increase the quantum yield of the LDS layer, the QDs are suspended in a polymer matrix which increases the interparticle distance between the QDs and reduces FRET. QDs can be dispersed in poly(methyl methacrylate) (PMMA) and poly(acrylic acid) (PAA), both of which are transparent in the UV from 300 to 400 nm. The QY of the polymer/QD film embedded in PMMA is 45% in air. We calculate the QD loading fraction by volume to be 6% using the band edge extinction coefficient (see Supporting Information).[12] Patterning of the LDS layer can be achieved if a resist such as PMMA is used.[13]

Figure 3 shows the measured external quantum efficiency (EQE) spectrum of an InGaAs photodiode before and after deposition of a ~1.2 μm thick LDS layer of PbS/CdS QDs embedded in PMMA. The EQE spectrum of the QD LDS detector shows an average

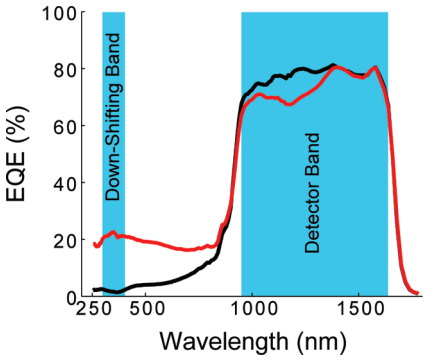

Figure 3. The efficiency of an InGaAs detector before (black line) and after addition of a PbS/CdS based LDS layer (red line). The average efficiency in the near UV (300–400 nm) is increased from 1.8% to 21%. The average efficiency in the infrared detector band decreases by 4.5%.

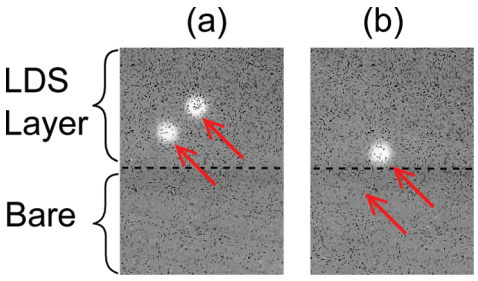

Figure 4. Images of two UV LEDs taken with an InGaAs SWIR imaging array. A UV transparent slide coated with a QD LDS layer covers the top half of the detector. (a) Both LEDs focused on the LDS layer. A strong response is observed from both LEDs. (b) QD LEDs translated such that only one LED focuses on the LDS layer. No response was observed from the LED incident on the bare detector.

12-fold enhancement of the EQE in the near UV (300–400 nm) from 1.8% to 21% after deposition of the QDs. The decrease in EQE below 300 nm is due to absorption by PMMA.

UV Imaging with SWIR Camera. Figure 4 shows two images taken with an InGaAs SWIR imaging array from Raytheon Vision Systems. The imaging array is partially covered with a UV grade fused silica slide coated with PbS/CdS QDs in PMMA. The light from two 285 nm emitting UV LEDs is collected by a UV transparent lens and imaged onto the camera. In Figure 4a, the light from both LEDs is incident on the QD coated slide, and the down-shifted light is detected by the camera. Figure 4b shows an image taken with the UV lights positioned such that the light from one LED is incident on the bare detector and the other on the QD coated slide. A large increase in UV sensitivity due to the LDS layer is clearly observed.

Bandwidth. The bandwidth of the LDS detector determines the maximum frame rate for imaging and the maximum frequency for communication. Infrared light that is not absorbed by the LDS layer will be detected at the bandwidth of the bare detector. The UV bandwidth of the LDS detector will be dominated by the delay

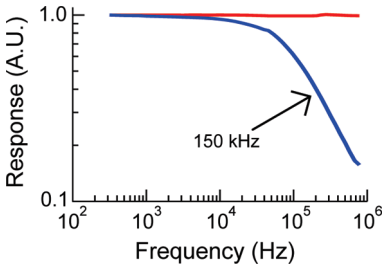

Figure 5. Bandwidth of an LDS detector containing PbS/CdS QDs measured under 1550 nm excitation (red line) and 365 nm excitation (blue line). A decrease in bandwidth to 150 kHz under UV excitation occurs due to the 1 μs photoluminescent lifetime of the QDs.

between absorption and re-emission of photons which is determined by the QD photoluminescent lifetime, τ_{PL}. For a single exponential photoluminescent decay, the frequency response $\Omega_L(f)$ is given by eq 1. The bandwidth is defined as the corner frequency, $f_c = 1/(2\pi\tau_{PL})$.

$$\Omega_L(f) = \frac{1}{\sqrt{1+(2\pi\tau_{PL}f)^2}} = \frac{1}{\sqrt{1+\left(\frac{f}{f_c}\right)^2}} \quad (1)$$

Fluorescent dye lifetimes are typically on the order of ~1 to 5 ns,[14] while quantum dot lifetimes vary from ~25 ns for CdSe[15] to ~1 μs for PbS and PbSe QDs.[16,17] The longer lifetime for lead chalcogenide QDs compared to CdSe QDs has been attributed to the higher dielectric constant[16] and higher 1S state degeneracy[17] in PbS and PbSe.

Figure 5 shows the measured bandwidth of an LDS detector made with PbS/CdS QDs in a PMMA matrix under UV excitation and SWIR excitation. The bandwidth of the underlying InGaAs photodiode is rated at 35 MHz. The response of the LDS detector to 1550 nm excitation is flat up to 1 MHz as expected since SWIR photons are not absorbed in the LDS layer. The UV response of the LDS detector rolls off at 150 kHz and the lifetime extracted from eq 1 is 1.1 μs which is consistent with the fluorescent lifetime of PbS QDs.[18,19]

Cross Talk. Optical cross talk occurs when light directed toward a given pixel by the imaging optics ultimately strikes a different pixel and leads to a loss in imaging resolution.[20,21] For a bare detector, optical cross talk results from reflection and scattering. Here we consider the increase in optical cross talk due to absorption and re-emission of photons in the LDS layer. Light that is not absorbed in the LDS layer will be detected with the same imaging resolution as the bare detector. For the PbS/CdS-based LDS detectors minimal infrared light is absorbed in the LDS layer so minimal loss of spatial resolution occurs in the detector band. However, light absorbed in the LDS layer is re-emitted isotropically and may travel a significant distance away from the spot of emission before being detected.

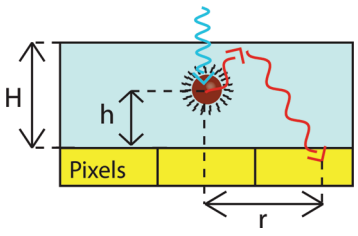

Figure 6. Cartoon of optical crosstalk due to the LDS layer.

We characterize the resolution of the LDS layer by $R_P(H)$, the radius from the emitter within which P percent of the photons strike the detector for an LDS film of height H. $R_P(H)$ can be derived from the intensity distribution of photons striking the detector at distance r from an emitter at height h above the detector (Figure 6). In the Supporting Information, we give the analytical intensity distribution for the limiting cases of low and high absorption of incident light by the LDS layer. It can be shown that in both cases, as $P \rightarrow 1$, R_P can be expressed by eq 2.

$$R_P(H) \approx \frac{H}{1-P} \quad (2)$$

For the case of R_σ, where $\sigma = 68\%$ and $R_{2\sigma}$, where $2\sigma = 95\%$, the resolution is $R_\sigma \approx 3H$ and $R_{2\sigma} \approx 20H$. For an LDS layer under 1 μm in height and a pixel size of 20 μm, the optical crosstalk is limited to adjacent pixels.

DISCUSSION

Modeling the EQE Spectrum. We present a simple model that explains the measured EQE spectrum of the LDS detector using the solution phase absorption and emission spectra. The EQE of the LDS detector at a specific wavelength, $\eta(\lambda)$, is given by eq 3 in terms of the EQE of the bare detector, $\eta_B(\lambda)$, the fraction of incident light absorbed in the LDS layer, $A(\lambda)$, the maximum external quantum efficiency of the bare detector, max(η_B), and the intrinsic LDS layer efficiency, η_L.

$$\eta(\lambda) = [1 - A(\lambda)]\eta_B(\lambda) + A(\lambda)\cdot\eta_L\cdot\max(\eta_B) \quad (3)$$

η_L is the normalized probability that a photon absorbed by the QDs in the LDS layer will ultimately generate an electrical signal in the detector. It is normalized by the maximum EQE of the bare detector so that an ideal LDS layer will have $\eta_L = 1$ regardless of the efficiency of the bare detector. Equation 4 gives η_L as a function of the quantum yield of the fluorophore, QY, the emission overlap integral, Θ_{Em}, and the collection efficiency, CE.

$$\eta_L = \mathrm{QY}\cdot\mathrm{CE}\cdot\Theta_{Em} \quad (4)$$

The emission overlap integral characterizes the overlap between the QD emission and the SWIR detection band. It is expressed in terms of the normalized emission profile of the fluorophore, $P_{em}(\lambda)$, and the

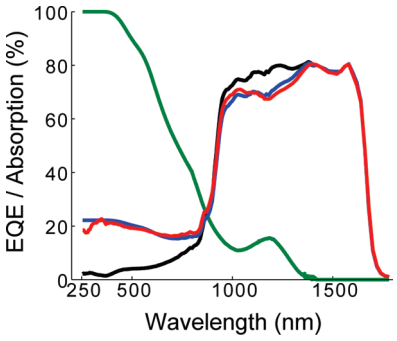

Figure 7. The efficiency of an InGaAs detector before (black line) and after addition of a PbS/CdS based LDS layer (red line). The LDS detector efficiency is fit (blue line) using eqs 3 to 5 and the scaled solution phase absorption profile of the QDs (green line). The experimental data are fit using an LDS layer efficiency of η_L = 28%.

normalized EQE of the bare detector by eq 5. For fluorophores with emission overlapping the detector band, Θ_{Em} will be near unity

$$\Theta_{Em} = \int P_{em}(\lambda) \frac{\eta_B}{\max(\eta_B)} d\lambda \qquad (5)$$

The collection efficiency, CE, factors in losses due to reabsorption and light emitted away from the detector. For simplicity, we consider the case of zero reabsorption of photons in the LDS layer. This is a reasonable approximation for our QD system due to the high SWIR transparency of the LDS layer. Since the QDs emit isotropically, 50% of the light will be emitted away from the detector. The amount that is reflected at the air−LDS layer interface will depend on the index of refraction of the LDS layer and can be modeled by the Fresnel equations. For an LDS layer with a refractive index of 1.45, approximately the index of PMMA in the SWIR, the ideal collection efficiency is estimated to be 87%. The actual CE will be reduced by surface roughness and reabsorption.

Equations 3 to 5 present a simple model for the wavelength dependent efficiency of the LDS detector. In Figure 7 this model is used to fit the measured EQE spectrum of an LDS detector. The fit is obtained by varying the magnitude of the QD absorption spectrum and the LDS layer efficiency, η_L. A good fit for both the EQE enhancement in the down-shifting band and the EQE decrease in the detector band is obtained for η_L = 28%. The value of the emission overlap integral is near unity, so the LDS layer efficiency is determined by the QY and collection efficiency. The 28% efficiency from the fit is lower than the value of 39% obtained using the measured 45% QY of the QDs in PMMA and the ideal collection efficiency of 87%. The difference can be accounted by assuming a lower than ideal collection efficiency and a reasonable error in the QY measurement. For example, a collection efficiency of 70% and a QY of 40% is consistent with the measured LDS layer efficiency.

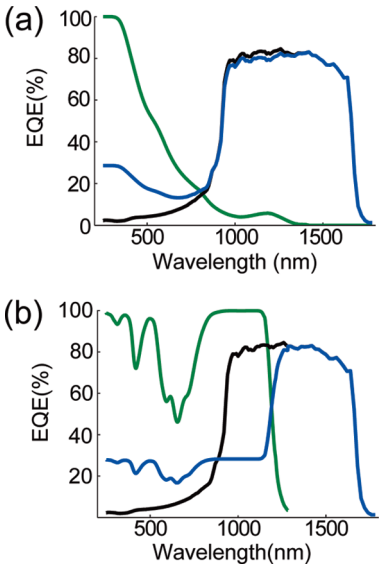

Figure 8. (a) Calculated efficiency of an LDS detector based on the absorption profile (green line) of PbS/CdS QDs. The predicted performance of the LDS detector (blue line) is compared to the bare detector (black line). A collection efficiency of 87% is assumed, and the absorption is set such that 95% of the incoming light is absorbed between 300 and 400 nm. (b) An equivalent calculation is done for Q Switch 5, a common SWIR fluorescent dye. Since the strongest absorption is at the HOMO−LUMO transition, the dye-based LDS layer absorbs nearly 100% of the incoming light across much of the detector band leading to a loss in SWIR performance.

Absorption Profile. The strong UV absorption of the QDs allows the QD LDS detector to absorb nearly all of the UV light without significant absorption in the infrared region. The effect of different absorption profiles is illustrated in Figure 8, which compares the numerically calculated LDS detector efficiencies of a QD (Figure 8a) and organic dye (Figure 8b) based LDS layer. Both the QD and dye (Q Switch 5, Exciton Dye Source) have a highest occupied molecular orbital-to-lowest unoccupied molecular orbital (HOMO−LUMO) transition at 1200 nm, and the LDS detector efficiency is calculated using a CE of 87% and a 40% QY for the QD and dye.

The absorption spectra are scaled so that the LDS layers absorb 95% of the incoming light between 300 and 400 nm. For the organic dye, the maximum absorption occurs at the HOMO−LUMO transition. To achieve strong absorption in the UV, the concentration of the dye in the LDS layer must be increased until the absorption at the HOMO−LUMO transition approaches 100%. Infrared light that would be collected at high efficiency by the detector is absorbed in the dye layer, and the detector band efficiency decreases significantly. A fluorophore with absorption to the blue of the detector band may be chosen to minimize this loss, however the emission of the fluorophore must overlap with the detector band. This requires a dye with a large Stokes shift and precise alignment of the dye spectrum with the detector band.

TABLE 1. Figure of Merit Values for Several SWIR Emitting Fluorphores[a]

Fluorophore	QY (%)	Θ_{em}	$T_{95}(\lambda_{DS})$
PbS/CdS QD	55	0.97	0.97
Q Switch 5	0.05	0.99	0.63
Cardiogreen	13	0.38	0.99

[a] Red boxes indicate critical areas of poor performance, and green boxes indicate near ideal perfomance. Values are calculated using the solution phase absorption spectrum, emission spectrum, and quantum yield. The down-shifting band, λ_{DS}, is 300−400 nm.

For QDs the molar extinction coefficient increases to the blue of the HOMO−LUMO transition. For the PbS/CdS QDs used in this study, the average molar extinction coefficient in the down-shifting band is ~60 times higher than the maximum molar extinction coefficient in the detector band. This can be used to create an LDS layer that is both highly absorptive in the down-shifting band and highly transparent in the detector band without requiring a large Stokes shift. This effect can be increased by the growth of a core/shell structure where the shell material does not absorb in the detector band. The shell serves as an optical antenna to absorb photons in the UV and transfer the exciton to the core material.

Figure of Merit Comparison. The quantum yield and emission overlap integral provide figures of merit for the emission properties of the fluorophore. We propose a figure of merit for the absorption profile of a fluorophore that characterizes its transparency in the detector band for a given average absorption in the down-shifting band. The detector band transparency, $T_A(\lambda_{DS})$, is the percentage of photons in the detector band that pass through the LDS layer without being absorbed. $T_A(\lambda_{DS})$ is given for an average absorption, A, across the down-shifting band, λ_{DS}. $T_A(\lambda_{DS})$ can be calculated from the absorption spectrum of the fluorophore and the EQE spectrum of the bare detector (see Supporting Information). For example, in the numerical calculation shown in Figure 8, $T_{95}(300-400)$ is 97% for the PbS/CdS QDs and 63% for the Q Switch 5 dye.

Table 1 presents figure of merit values for the PbS/CdS QDs used above and two SWIR emitting dyes (Q Switch 5 and Cardiogreen). Red squares indicate the critical areas of poor performance and green squares indicate near ideal performance. The organic dye QY values are too low for use in practical UV−SWIR LDS applications. In addition, for the organic dyes the strong absorption at the HOMO−LUMO transition makes it difficult to achieve both strong overlap of the emission with the detector band and weak overlap of the absorption with the detector band. The current limitation for QD based UV−SWIR LDS detectors is clearly the quantum yield. The LDS detector efficiency is calculated for different QY values in Figure 9, assuming a collection efficiency of 87%. Given the recent advances in high QY visibly emitting QDs where QY values above 95% are obtained,[22] it is plausible that QD based UV−SWIR LDS detectors with down-shifting band efficiencies greater than 50% will be achievable using the architecture presented here as synthetic progress is made with high QY SWIR emitting QDs.

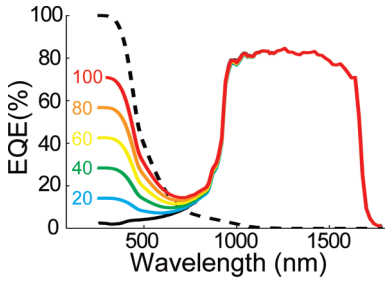

Figure 9. Calculated EQE spectra of a PbS/CdS QD-based LDS detector for different QY values (colored lines) compared to the bare detector (solid black line). The solution phase absorption spectrum (dashed black line) is from PbS/CdS QDs with a band edge at 950 nm and is scaled so 95% of the incoming light is absorbed between 300 and 400 nm. A collection effieciency of 87% is used.

CONCLUSION

We have presented a method to sensitize SWIR detectors to UV light using colloidal quantum dots. A 21% average EQE in the near UV is obtained with a 4.5% average loss of SWIR sensitivity. This is made possible by the high SWIR QY and unique absorption profile of the QDs. We give a simple model for the efficiency of the LDS detector which fits the observed EQE spectra. The UV bandwidth of the LDS detector is shown to determined by the photoluminescent lifetime, and a simple model for the optical cross talk created by the LDS layer is presented.

METHODS

PbS/CdS core/shell nanocrystals were synthesized using a large scale method based on previous procedures (see Supporting Information).[9,23]

A 6% PMMA solution in chlorobenzene was prepared by sonication of 120 000 MW PMMA (Sigma Aldrich) in chlorobenzene. Films were either drop cast or spin-coated at 1500 rpm for 60 s. Film thickness was measured using a Veeco Dektak 6 M Stylus Profiler.

Absorption measurements where performed with a Carey 5000 UV−vis−NIR spectrometer. For solution phase measurements trichlorotrifluoroethane was used as a infrared transparent solvent.

Emission spectra were taken using a Princeton Instruments Spectra Pro 300i spectrometer coupled to a Princeton Instruments OMA V InGaAs CCD array detector. The excitation source was a 632 HeNe laser, and the scattered excitation light was blocked with an 850 nm long pass filter.

InGaAs photodiodes were used as purchased from Hamamatsu Corporation, part number G8941-01. Electrical contact was made to the anode and cathode *via* silver paint, and the samples were mounted on a glass substrate.

External quantum efficiency measurements were taken using a Spectra Pro SP2150 equipped with a xenon arc lamp to generate monochromatic light from 250 to 2000 nm. The excitation intensity in the visible was measured with a calibrated Newport 818-UV enhanced Si photodiode and in the infrared with a calibrated Newport 818-IR Ge photodiode. For each spectral region, appropriate long pass and short pass filters were used to isolate the monochromatic light. Short pass filters are particularly important for accurate measurements in the UV portion of the spectrum. Aluminum mirrors were used instead of lenses to prevent chromatic aberration over the broad spectral range used. To remove error due to waveguiding and the difference in size between the LDS detector and the reference detectors, the EQE is also measured using a focused 1550 nm laser with a spot size less than 250 μm. The absolute magnitude of the EQE spectrum taken with the spectrometer is scaled to match the EQE taken at 1550 nm.

The quantum yield measurements are described in detail in the Supporting Information. Absolute quantum yield measurements are made using an integrating sphere and calibrated reference detectors.

Acknowledgment. This work was supported in part by the U. S. Army through the Institute for Soldier Nanotechnologies (W911NF-07-D-004). S. Geyer acknowledges support from the Corning Foundation and the Martin Family Society of Fellows for Sustainability. The authors gratefully acknowledge the following people at Raytheon Vision Systems: David Acton for use of the SWIR lab, Scott Taylor for consultations on readout integrated circuit operation, John de Loo for the mechanical structures used for down-shifting plates, and Jessica Wyles for operating the SWIR camera, technical support and image processing.

Supporting Information Available: Quantum dot synthesis, quantum yield measurements, quantum yield stability, calculation of QD volume fraction, and mathematical analysis of cross talk and detector band transparency. This material is available free of charge *via* the Internet at http://pubs.acs.org.

REFERENCES AND NOTES

1. Klampaftis, E.; Ross, D.; McIntosh, K. R.; Richards, B. S. Enhancing the Performance of Solar Cells *via* Luminescent Down-Shifting of the Incident Spectrum: A Review. *Sol. Energy Mater. Sol. Cells* **2009**, *93*, 1182–1194.
2. Ariyawansa, G.; Rinzan, M. B. M.; Alevli, M.; Strassburg, M.; Dietz, N.; Perera, A. G. U.; Matsik, S. G.; Asghar, A.; Ferguson, I. T.; Luo, H.; *et al*. GaN/AlGaN Ultraviolet/Infrared Dual-Band Detector. *Appl. Phys. Lett.* **2006**, *89*, 091113–3.
3. Jayasinghe, R. C.; Ariyawansa, G.; Dietz, N.; Perera, A. G. U.; Matsik, S. G.; Yu, H. B.; Ferguson, I. T.; Bezinger, A.; Laframboise, S. R.; Buchanan, M.; *et al*. Simultaneous Detection of Ultraviolet and Infrared Radiation in a Single GaN/GaAlN Heterojunction. *Opt. Lett.* **2008**, *33*, 2422–2424.
4. Ariyawansa, G.; Perera, A. G. U.; Huang, G.; Bhattacharya, P. Wavelength Agile Superlattice Quantum Dot Infrared Photodetector. *Appl. Phys. Lett.* **2009**, *94*, 131109–3.
5. Starikov, D.; Boney, C.; Pillai, R.; Bensaoula, A. Dual-Band UV/IR Optical Sensors for Fire and Flame Detection and Target Recognition. *Sens. Ind. Conf., Proc. ISA/IEEE* **2004**, 36–40.
6. Slooff, L. H.; Kinderman, R.; Burgers, A. R.; Bakker, N. J.; van Roosmalen, J. A. M.; Buchtemann, A.; Danz, R.; Schleusener, M. Efficiency Enhancement of Solar Cells by Application of a Polymer Coating Containing a Luminescent Dye. *J. Sol. Energy Eng.* **2007**, *129*, 272–276.
7. Gallagher, S. J.; Norton, B.; Eames, P. C. Quantum Dot Solar Concentrators: Electrical Conversion Efficiencies and Comparative Concentrating Factors of Fabricated Devices. *Sol. Energy* **2007**, *81*, 813–821.
8. Chatten, A. J.; Barnham, K. W. J.; Buxton, B. F.; Ekins-Daukes, N. J.; Malik, M. A. A New Approach to Modelling Quantum Dot Concentrators. *Sol. Energy Mater. Sol. Cells* **2003**, *75*, 363–371.
9. Pietryga, J.; Werder, D.; Williams, D.; Casson, J.; Schaller, R.; Klimov, V.; Hollingworth, J. Utilizing the Lability of Lead Selenide to Produce Heterostructured Nanocrystals with Bright, Stable Infrared Emission. *J. Am. Chem. Soc.* **2008**, *130*, 4879–4885.
10. Kagan, C. R.; Murray, C. B.; Nirmal, M.; Bawendi, M. G. Electronic Energy Transfer in CdSe Quantum Dot Solids. *Phys. Rev. Lett.* **1996**, *76*, 1517–1520.
11. Bose, R.; McMillan, J. F.; Gao, J.; Rickey, K. M.; Chen, C. J.; Talapin, D. V.; Murray, C. B.; Wong, C. W. Temperature-Tuning of Near-Infrared Monodisperse Quantum Dot Solids at 1.5 μm for Controllable Forster Energy Transfer. *Nano Lett.* **2008**, *8*, 2006–2011.
12. Cademartiri, L.; Montanari, E.; Calestani, G.; Migliori, A.; Guagliardi, A.; Ozin, G. A. Size-Dependent Extinction Coefficients of PbS Quantum Dots. *J. Am. Chem. Soc.* **2006**, *128*, 10337–10346.
13. Martiradonna, L.; Stomeo, T.; Giorgi, M. D.; Cingolani, R.; Vittorio, M. D. Nanopatterning of Colloidal Nanocrystals Emitters Dispersed in a PMMA Matrix by e-Beam Lithography. *Microelectron. Eng.* **2006**, *83*, 1478–1481.
14. Resch-Genger, U.; Grabolle, M.; Cavaliere-Jaricot, S.; Nitschke, R.; Nann, T. Quantum Dots *versus* Organic Dyes as Fluorescent Labels. *Nat. Meth.* **2008**, *5*, 763–775.
15. Fisher, B. R.; Eisler, H.-J.; Stott, N. E.; Bawendi, M. G. Emission Intensity Dependence and Single-Exponential Behavior in Single Colloidal Quantum Dot Fluorescence Lifetimes. *J. Phys. Chem. B* **2003**, *108*, 143–148.
16. Wehrenberg, B. L.; Wang, C.; Guyot-Sionnest, P. Interband and Intraband Optical Studies of PbSe Colloidal Quantum Dots. *J. Phys. Chem. B* **2002**, *106*, 10634–10640.
17. An, J. M.; Franceschetti, A.; Zunger, A. The Excitonic Exchange Splitting and Radiative Lifetime in PbSe Quantum Dots. *Nano Lett.* **2007**, *7*, 2129–2135.
18. Warner, J. H.; Thomsen, E.; Watt, A. R.; Heckenberg, N. R.; Rubinsztein-Dunlop, H. Time-Resolved Photoluminescence Spectroscopy of Ligand-Capped PbS Nanocrystals. *Nanotechnology* **2005**, *16*, 175.
19. Cademartiri, L.; Bertolotti, J.; Sapienza, R.; Wiersma, D. S.; von Freymann, G.; Ozin, G. A. Multigram Scale, Solventless, and Diffusion-Controlled Route to Highly Monodisperse PbS Nanocrystals. *J. Phys. Chem. B* **2006**, *110*, 671–673.
20. Younger, R. D.; McIntosh, K. A.; Chludzinski, J. W.; Oakley, D. C.; Mahoney, L. J.; Funk, J. E.; Donnelly, J. P.; Verghese, S. Crosstalk Analysis of Integrated Geiger-Mode Avalanche Photodiode Focal Plane Arrays. *Advanced Photon Counting Techniques III*; SPIE: Bellingham, WA, 2009; Vol. 7320, No. 73200Q-12.
21. Holloway, H. Collection Efficiency and Crosstalk in Closely Spaced Photodiode Arrays. *J. Appl. Phys.* **1986**, *60*, 1091–1096.
22. Liu, W.; Greytak, A. B.; Lee, J.; Wong, C. R.; Park, J.; Marshall, L. F.; Jiang, W.; Curtin, P. N.; Ting, A. Y.; Nocera, D. G.; *et al*. Compact Biocompatible Quantum Dots *via* RAFT-Mediated Synthesis of Imidazole-Based Random Copolymer Ligand. *J. Am. Chem. Soc.* **2010**, *132*, 472–483.
23. Hines, M.; Scholes, G. Colloidal PbS Nanocrystals with Size-Tunable Near-Infrared Emission: Observation of Post-synthesis Self-Narrowing of the Particle Size Distribution. *Adv. Mater.* **2003**, *15*, 1844–1849.